Impact of Approximate DFT Density Delocalization Error on Potential Energy Surfaces in Transition Metal Chemistry

Fang Liu[1] and Heather J. Kulik[1,*]

[1]*Department of Chemical Engineering, Massachusetts Institute of Technology, Cambridge, MA 02139*

ABSTRACT: For approximate density functional theory (DFT) to be useful in catalytic applications of transition metal complexes, modeling strategies must simultaneously address electronic, geometric, and energetic properties of the relevant species. We show that for representative transition metal triatomics (MO_2, where M = Cr, Mn, Fe, Co, or Ni) and related diatomics the incorporation of Hartree–Fock (HF) exchange in most cases improves the properties of the Born–Oppenheimer potential energy surface (PES) with respect to accurate experimental or CCSD(T) references. We rationalize this observation by noting reduced delocalization obtained with hybrid functionals (20–40% HF exchange), as evidenced by reduced hybridization of non-bonding orbitals and increases in metal partial charges. Although we show that the optimal exchange fraction is both property and system specific, incorporating HF exchange synergistically improves properties of density, structure, and energetics within a single PES characterized by moderately covalent bonding. The same improvement is not observed in the ordering of MO_2 spin states, as good agreement of semi-local DFT spin state ordering is worsened by over-stabilization of higher spin states when HF exchange is added. More work is needed to understand minimal functional forms capable of improving multiple properties with respect to semi-local DFT descriptions of transition metal chemistry.

1. Introduction

Accurate modeling of transition metal chemistry is central to advancing fundamental understanding in catalysis and materials science. Although density functional theory (DFT) is widely employed in computational chemistry for its balance of cost and accuracy in main group chemistry, most exchange-correlation (xc) approximations in DFT suffer from one- and many-electron self-interaction errors[1-5], commonly referred to as delocalization error[6-8] (DE). As DEs are commonly imbalanced across the structures being compared, DE can erode DFT predictions of common properties, such as electron affinities[9-11], band gaps[12-13], barrier heights[14], and dissociation energies[2, 15-18]. The valence (i.e., *d* or *f*) electrons of open shell transition metal complexes are particularly sensitive to DE imbalances, leading to strongly xc-dependent predictions of spin-state[19-24] or magnetic ordering[25-27] and thus electronic properties. Although effort has been made to overcome some of these limitations through "higher rung" density functionals[28-33], semi-local generalized gradient approximation (GGA) DFT remains widely used in transition metal chemistry for its simplicity and low computational cost.

Common approaches to reducing DE imbalances in GGAs include the use of Hubbard U-corrected DFT (i.e., DFT+U[34-36]), hybrid functionals that introduce an admixture of Hartree–Fock (HF) exchange globally or with range separation[37-44]. A distinct approach[45-46] to these physically-motivated, few-parameter corrections is to increase the number of parameters in the functional and tune them to improve performance on predicting energetics of available reference data. Although physically-motivated tuning approaches exist for both DFT+U[19, 47-49] and hybrids[50-52], it is common practice to choose parameters that reproduce a handful of target energetic properties, reducing method selection to a data fitting procedure[53]. For transition metal chemistry and catalysis, this approach is challenged both by the availability of reference data and

the highly system- or property-specific nature of optimal functional choice[20-22, 54-60].

An open question remains whether it is possible to simultaneously improve multiple properties[61] within a single, few parameter xc functional or if improving one error (e.g., energetic DE) must worsen another (e.g., static correlation error[62-64]). It has been well known for some time that some xcs that provide good energetics yield poor densities in comparison to accurate references[65], whereas others yield poor energetics and good densities[66], as has been borne out by more recent observations on charged ions and small organic molecules[67-71]. However, non-self-consistent replacement of approximate DFT densities with localized ones derived from HF theory have been demonstrated to yield improved barrier heights[72-73] and dissociation energies[6, 74-75], enabling a separation of energetic- and density-driven DEs[6]. The relationship between density and energetic errors in transition metal chemistry is less clear[76-82]. Eliminating energetic DE in transition metal complexes does not eliminate density DE with respect to accurate wavefunction theory references[76]. Methods that approximately correct energetic DE can have divergent effects on densities[83] and surface properties[84] in correlated, transition metal oxide solids.

As a representative example, transition metal dioxides (MO_2) in the inserted structure represent an interesting test case for understanding the interplay between density and geometric errors in electronic structure methods.[85] Experimentally[86-93] mid-row 3*d* transition metal dioxides (e.g., Cr, Mn, Fe) are bent with acute angles, and increasing *d* filling leads to increasing ∠(O-M-O) angles with linear structures favored for later (e.g., Co or Ni) transition metals (Figure 1). This variation can be interpreted as a change from a double-well angular potential with ∠(O-M-O) = 180° as a local maximum to a single-well potential with the linear structure at a minimum (Figure 1). Semi-local (i.e., GGA) functionals with plane wave (PW) basis sets underestimate

∠(O-M-O) and prefer bent structures even for experimentally linear MO_2 molecules (e.g., CoO_2)[85]. DE correction with DFT+U[34-36] has been shown to overcompensate and favor linear structures for earlier (e.g., Mn) transition metals[85], both through corrections to the density and through M-O bond over-elongation.

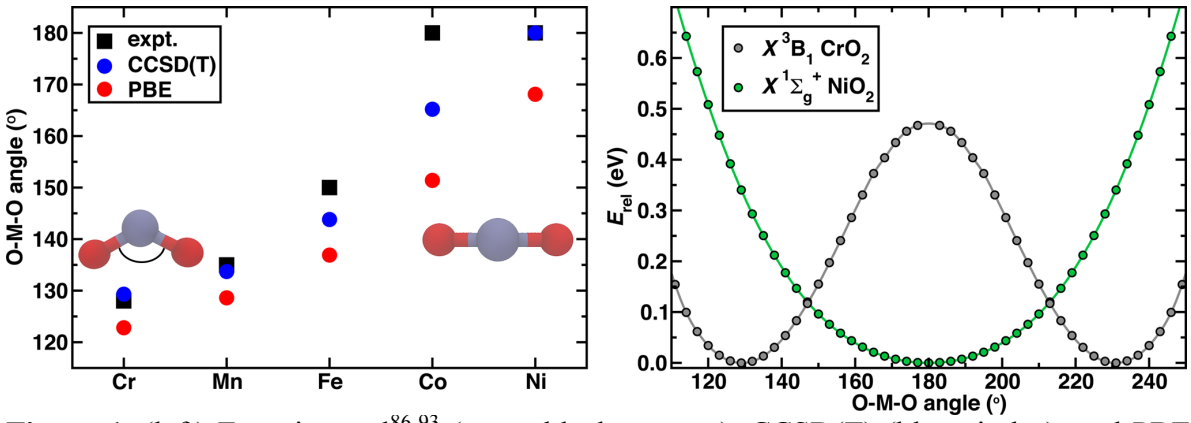

Figure 1. (left) Experimental[86-93] (expt., black squares), CCSD(T) (blue circles), and PBE (red circles) ∠(O-M-O) (in °) for the ground state MO_2 molecules (M = Cr, Mn, Fe, Co, or Ni from left to right in the plot, as indicated on axis). The angle is annotated on a representative bent molecule in the left structural inset, and a linear molecule is also shown for reference with the metal atom shown in gray and the oxygen atoms shown in red. (right) Overlay of the potential energy curves (E_{rel}, in eV) from the CCSD(T) $X\,^3B_1$ CrO_2 (grey circles) double-well potential and CCSD(T) $X\,^1\Sigma_g^+$ NiO_2 (green circles) single-well potential with respect to the O-M-O angle (in °), with both curves aligned so that their minima are assigned zero. A cubic spline of the data is also shown.

Although MO_2 molecular properties have been shown to be improved[85] with inter-site extensions[94] to DFT+U or with quantum Monte Carlo[95], the extent to which hybrid functionals can improve upon GGA descriptions of MO_2 molecules is not known. In this work, we study the effect of DE tuning by hybrid functionals on density, geometry, and energetic properties in representative transition metal triatomics to determine if synergistic improvements can be obtained for multiple properties with respect to experiment and accurate wavefunction theory references. The rest of this work is as follows. In Section 2, we describe the Computational Details of the calculations in this work. In Section 3, we present the Results and Discussion on five transition metal dioxides and provide a comparison to observations on related diatomic

molecules. Finally, in Section 4, we provide our Conclusions.

2. Computational Details

Transition Metal Dioxides. Transition metal dioxide (MO_2, M = Cr, Mn, Fe, Co, or Ni) structures were studied in an inserted geometry (i.e., O-M-O). We studied experimentally observed[86-93] ground and low-lying electronic states of each MO_2 molecule, i.e., CrO_2[86]: ground state, $X\,^3B_1$ and $^1A_1$; MnO_2[87-88]: $X\,^4B_1$ and $^2B_1$; FeO_2[89-90]: $X\,^3B_1$, $^1A_1$, and $^5B_2$; CoO_2[91-92]: $X\,^2\Delta_g$, $^4A_2$, and $^6A_1$; NiO_2[93]: $X\,^1\Sigma_g^+$, $^3A_2$, and $^5A_1$. Symmetry was not enforced on the wavefunction during electronic structure calculations, and term symbol assignment was instead verified by visual inspection of orbitals. For these molecules with C_{2v} symmetry, two internal degrees of freedom were varied in potential energy scans or geometry optimizations: the metal–oxygen bond length ($d_{M\text{-}O}$) and O-M-O angle ($\angle$(O-M-O)). For the potential energy scan, $\angle$(O-M-O) was varied from 108 to 180° in 3° increments for single point energy evaluation at fixed $d_{M\text{-}O}$ on structures generated by an in-house Python script. Select numerical harmonic frequencies were computed for $X\,^4B_1$ MnO_2 (Supporting Information Text S1).

Diatomic Molecules. The lowest energy $^6\Sigma^+$ state of a series of isoelectronic diatomic molecules, CrF, CrO^-, MnO, FeO^+, and FeN, was characterized, which in most cases is the experimentally-characterized ground state[88, 96-103]. Equilibrium bond lengths were obtained from a DFT geometry optimization, and potential energy curves (PECs) were obtained for all methods by displacing the bond by up to 0.1 Å in either direction in 0.002 Å increments. Numerical harmonic frequencies were obtained from a linear fit to the first derivative of the energy at equilibrium and had good agreement with analytical frequencies (Supporting Information Table S1 and Text S1). Bond dissociation energies, D_e, were evaluated as the electronic energy difference between the PEC minimum and the energies of the isolated species, which were

selected based on the most stable isolated species (Supporting Information Table S2). The PEC energies and D_e values were used to fit a Morse potential in xmgrace with only the force constant treated as an adjustable parameter.

DFT Calculations. DFT calculations, both single point energies and geometry optimizations, were carried out in ORCA v.4.0.0.2[104] with the PBE[105] GGA functional. The def2-TZVP basis set[106] was chosen after testing convergence of geometric properties (Supporting Information Figure S1). The HF exchange fraction, a_{HF}, was varied in a PBE0[107]-like form from as low as 0.0 (i.e., pure PBE) to as high as 0.4 in 0.1 or 0.2 increments (see Sec. 3). Geometry optimizations were carried out using BFGS[108-113] in redundant internal coordinates implemented to the default tolerances of 3×10^{-4} hartree/bohr for the maximum gradient and 5×10^{-6} hartree for the change in energy between steps. Only singlets were calculated in a restricted formalism. As in prior work[22, 24, 29, 54], exchange sensitivities of relevant geometric and energetic properties, p, were computed as linear approximations:

$$\frac{\partial p}{\partial a_{HF}} \approx \frac{\Delta p}{\Delta a_{HF}} \tag{1}$$

which generally holds well across the a_{HF} = 0.0 to 0.4 range, as indicated by values of $R^2 > 0.9$. In addition to reporting sensitivities in terms of property change with unit HF exchange variation (i.e., HFX), we used these expressions to interpolate the optimal a_{HF} to match reference values.

WFT References. Reference calculations for both MO_2 and $^6\Sigma^+$ diatomic molecules were obtained with coupled cluster singles and doubles with perturbative triples (CCSD(T)) theory using the def2-TZVP basis set[114-115] with ORCA v.4.0.0.2.[104] A frozen core treatment with default definitions ($1s^2$ for N, O, and F and $1s^22s^2p^6$ for metals) was employed throughout. Only singlets were calculated in a restricted formalism. For open-shell CCSD(T), an unrestricted HF (UHF) reference was used followed by transformation to quasi-restricted orbitals to remove spin

contamination. Multi-reference character was assessed using recommended[116] diagnostics of single amplitudes[117-119] (i.e., T_1 or D_1) and contribution of the triples term to the atomization energy[120] (%TAE). PECs were obtained at the CCSD(T) level for all $^6\Sigma^+$ diatomic molecules. For all MO_2 molecules and states, a CCSD(T) PEC was obtained using the $d_{M\text{-}O}$ obtained for that state with PBE, and ∠(O-M-O) was varied as for DFT PECs. For the experimental ground states of each MO_2 molecule, a 2D potential energy surface was also obtained (see Sec. 3 and Supporting Information Figures S2-S6). Numerical harmonic frequencies were also calculated for $X\,^4B_1$ MnO_2 with orb-opt CCSD(T), as described in the main text.

Density Analysis. Gaussian cube files (100×100×100 real space grid resolution; point spacing: 0.01 Å) were generated with the orca_plot code followed by numerical density averaging in Multiwfn[121]. For analysis of CCSD(T) wavefunctions, the orbital-optimized (orb-opt) CCSD(T) method[122-124] was employed to generate a density close to the fully relaxed one.[125] For the $^6\Sigma^+$ diatomics, the aug-cc-pVTZ basis was employed in the orb-opt CCSD(T) calculations to ensure balanced treatment of the relevant anion species (CrO^-), but this basis set size was intractable for the larger triatomic systems. Bader partial atomic charges[126] were obtained from higher resolution (401×401×401) grids, which were selected to ensure convergence, using the BADER[127] program (Supporting Information Figure S7).

3. Results and Discussion

3a. Structure and Density Errors in MO_2.

Here, we study the effect of tuning exchange in hybrid calculations on the low-lying states of five inserted transition metal dioxide MO_2 (M = Cr, Mn, Fe, Co, or Ni) structures that span the transition from bent to linear in experiments (Figure 1). We compare to available experimental ground state structural data and an accurate CCSD(T) reference for both ground

and low-lying state structural and density properties to determine if tuning density delocalization has an effect on experimentally-observable structural properties. We choose CCSD(T) for its good agreement with experimentally available[86-93] structures despite significant[116] multireference diagnostic[117-120] values for most states (Figure 1 and Supporting Information Table S3). Compared to CCSD(T) or experiment, localized-basis set PBE calculations systematically underestimate ∠(O-M-O) values across the MO_2 series, motivating further investigation (Figure 1).

3.a.1. MnO_2 Density and Structure.

The MnO_2 ground state (i.e., $X\,^4B_1$[87,88]) is an exemplary case where the PBE equilibrium ∠(O-Mn-O) is more acute (ca. 128°) than the experimental[87,88] value (135±5°), regardless of whether a PW[85] or localized basis set is employed (Figure 2 and Supporting Information Table S4). Incorporating HF exchange increases the equilibrium angle monotonically, producing a ∠(O-Mn-O) of 135° at a_{HF} = 0.4 that agrees with experiment (Supporting Information Tables S4 and S5). In these systems, DFT+U had been shown to also increase MO_2 molecule angles both through changes in density delocalization and through bond elongation (e.g., by 0.1 Å for $X\,^4B_1$ MnO_2).[85] Although hybrid tuning changes equilibrium $d_{Mn\text{-}O}$ by less than 0.01 Å, we primarily evaluate angular PECs obtained at fixed PBE $d_{M\text{-}O}$ values to isolate density delocalization from bond elongation effects on angular PEC changes (Supporting Information Table S5).

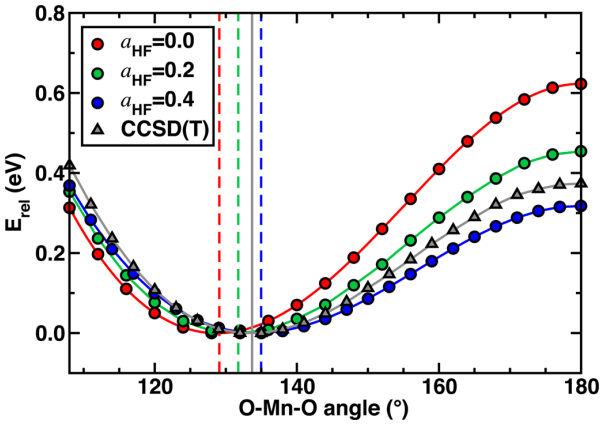

Figure 2. Angular PEC for the ground state $X\,^4B_1$ of MnO_2 with fixed $d_{Mn\text{-}O}$=1.59 Å. PECs are computed with PBE at three values of HF exchange, a_{HF} = 0.0 (red circles), 0.2 (green circles), and 0.4 (blue circles), along with the CCSD(T) reference (grey triangles). The optimal angle for each PEC is indicated for DFT (dashed lines) and CCSD(T) (solid line) following the same coloring scheme and as indicated in inset.

The increase in ∠(O-Mn-O) equilibrium value for the $X\,^4B_1$ MnO_2 angular PEC ($d_{Mn\text{-}O}$ = 1.59 Å) with HF exchange corresponds to a decreased stabilization of the bent structure over the linear (i.e., ΔE(linear-bent), see Figure 2 and Supporting Information Table S6). The ΔE(linear-bent) for a_{HF} = 0.4 (0.32 eV) is half of the a_{HF} = 0.0 value (0.62 eV), in good agreement with CCSD(T) (0.37 eV, Figure 2 and Supporting Information Table S6). Generalizing this PEC analysis to the vibrational modes of $X\,^4B_1$ MnO_2, improved agreement with CCSD(T) symmetric bend and stretch frequencies is achieved at high ($a_{HF} \geq 0.3$) exchange fractions, but all a_{HF} values systematically underestimate the CCSD(T) asymmetric stretch (Supporting Information Table S7). Consistent with prior analysis, stretching $d_{Mn\text{-}O}$ beyond the PBE equilibrium value in 0.1 Å increments to 1.69 Å and 1.79 Å produces significantly softer angular PECs with PBE ΔE(linear-bent) values reduced to 0.30 and 0.10 eV, respectively (Figure 3). Angular sensitivities also increase for these shallower PECs, with near-degenerate bent and linear structures at a_{HF} = 0.2 for $d_{Mn\text{-}O}$=1.79 Å and a linear structure favored at a_{HF} = 0.4 (Figure 3).

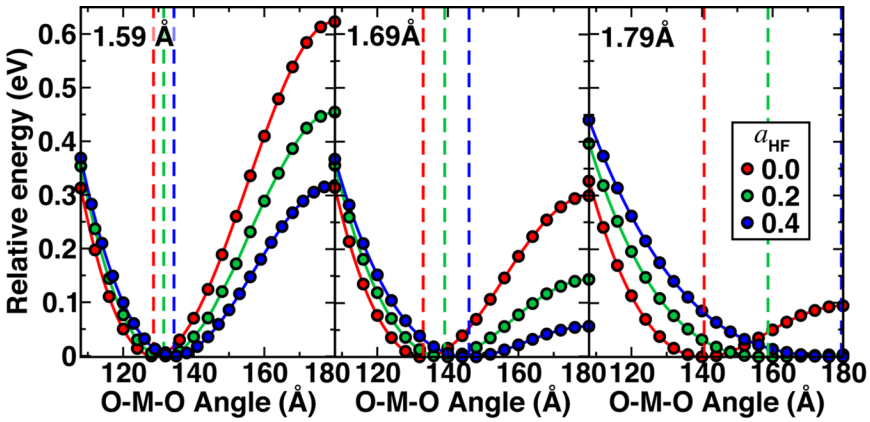

Figure 3. Angular PECs for $X\ ^4B_1$ MnO_2 at three values of $d_{Mn\text{-}O}$=1.59, 1.69, and 1.79 Å (from left to right) are computed with PBE for a_{HF} = 0.0 (red circles), 0.2 (green circles), and 0.4 (blue circles) values. The minimum energy angle for each PEC is labeled by a dashed vertical line of the same color, as also indicated in inset legend.

Trends consistent with the quartet ground state are found for the low-lying $^2B_1$ MnO_2 angular PEC ($d_{Mn\text{-}O}$ = 1.59 Å, Supporting Information Figure S8 and Table S4). Despite $^2B_1$ MnO_2 having a comparable PBE equilibrium ∠(O-Mn-O) of 128° with respect to ground state $X\ ^4B_1$, the shallower PBE PEC (ΔE(linear-bent) = 0.4 eV) produces a geometry more sensitive to HF exchange, with ∠(O-Mn-O) increasing by 10° to 138° for a_{HF} = 0.4, somewhat overestimating the CCSD(T) value (132°, Supporting Information Figure S8 and Table S4). The overall shape of the CCSD(T) angular PEC and ΔE(linear-bent) value (0.23 eV) for $^2B_1$ MnO_2 is intermediate between a_{HF} = 0.2 and 0.4 results (0.20-0.29 eV, Supporting Information Figure S8 and Table S6). MnO_2 energetic and structural property agreement with respect to CCSD(T) or experiment is broadly improved by incorporating 20-40% HF exchange.

We next consider whether changes in density delocalization, as have been previously invoked in DFT+U studies on MnO_2[85], could rationalize why incorporating HF exchange simultaneously improves DFT-level geometric and energetic property agreement with CCSD(T) reference (see Sec. 2). As in prior work[76, 83-84], we compute real space partial charges[126-127] with both DFT and CCSD(T) for an equilibrium structure of $X\ ^4B_1$ MnO_2 (Supporting Information

Table S5, Figure S3 and S9). The PBE Mn partial charge (q_{Mn} = 1.4 e) is a significant underestimate of the CCSD(T) value (q_{Mn} = 1.6 e), but incorporating high exchange fractions (a_{HF} = 0.4) that improve the DFT PEC also recover a q_{Mn} to close to the CCSD(T) value (Supporting Information Figure S9).

To further examine effects of hybrid tuning on the density, we revisit a proposal[85] that delocalization of density from nominally non-bonding δ-type transition metal d_{xy} or d_{x2-y2} orbitals through hybridization with oxygen 2*p* orbitals over-stabilizes bent structures with semi-local DFT (e.g., PBE). Examining the shapes of these δ orbitals in the $X\ ^4B_1$ state of MnO_2 with increasing HF exchange fixed at the PBE geometry (d_{Mn-O} =1.59 Å, ∠(O-Mn-O) =129°) confirms prior observations (Figure 4). The density along the non-bonded O···O midpoint in d_{x2-y2}-derived δ orbitals for PBE is systematically reduced with increasing a_{HF} (Figure 4). This change in the density leads to a solely metal-centered δ orbital in the spin-up case and oxygen-centered orbitals with no metal character for spin down (Figure 4). The d_{xy}-derived δ orbitals have less apparent delocalization of density through the O···O midpoint but broadly localize again to metal-centered for spin-up and oxygen-centered for spin-down orbitals with increasing a_{HF} (Figure 4). Although some differences remain (e.g., for the spin-up d_{x2-y2}-derived δ orbital), the a_{HF} = 0.4 orbitals are in the best agreement with those obtained from CCSD(T) at its equilibrium structure, consistent with the exchange fraction for which structure and energetic agreement was achieved (Figure 4 and Supporting Information Figure S10).

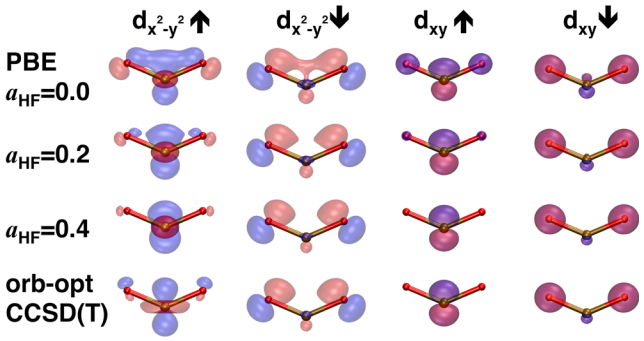

Figure 4. Depiction of $X\ ^4B_1$ MnO_2 MOs (isovalue: 0.01 e/bohr^3) derived from Mn $3d_{x2\text{-}y2}$ and $3d_{xy}$ hybridization with O *2p* states for three different values of a_{HF} compared to orb-opt CCSD(T). The orb-opt CCSD(T) orbitals were obtained at the CCSD(T) equilibrium geometry.

Thus far, we have focused on the synergistic relationship between qualitative corrections of density delocalization error with quantitative improvements in structural properties. To make the connection to energetic delocalization error (EDE i.e., deviation from piecewise linearity[47, 50, 128]), we evaluate how EDE is reduced by increasing a_{HF} and find hybrid tuning to improve but not eliminate EDE (Supporting Information Figure S11 and Table S8). An alternative approach to eliminating EDE is to tune[37-44] the range-separation parameter in a range-separated hybrid (RSH) functional with HF exchange in the long range. For $X\ ^4B_1$ MnO_2, we observe some improvements in the density with an RSH but insufficient PEC tuning, with minimal changes to the equilibrium PBE ∠(O-Mn-O) (Supporting Information Figures S12-S13). Simultaneous tuning of range separation and global exchange could be of interest in future work to identify if more adjustable parameters facilitate the simultaneous improvement of multiple properties.

3.a.2. Density and Structure in other MO_2 Molecules.

To generalize the structure–density observations from MnO_2, we extend our study to four other mid-row MO_2 molecules (M = Cr, Fe, Co, or Ni) in their low-lying states (details provided in Sec. 2). We compare angular PECs for all low-lying states with $d_{M\text{-}O}$ fixed to the ground state PBE equilibrium values, which have a narrow range (from 1.57 Å for CoO_2 to 1.60 Å for NiO_2,

see Supporting Information Tables S4-S5). In most cases (e.g., Cr, Mn, and Fe), this bond length is close (i.e., within 0.01-0.05 Å) to both the equilibrium value in other low-lying states and insensitive to increasing a_{HF} (Supporting Information Table S5). Differences in population of anti-bonding orbitals for high-spin states (e.g., quintet or sextet) over low- and intermediate-spin states in later transition metals (i.e., Co or Ni) leads to a wider range (ca. 0.1 Å) of equilibrium $d_{M\text{-}O}$ values across spin states and a_{HF} values (Supporting Information Table S5). However, given the observations on angular PECs in MnO_2 with varied M-O bond lengths, we can expect qualitative trends in angular PECs to hold (see Figure 3).

In almost all (12 of 13) cases, HF exchange increases ∠(O-M-O) monotonically, which broadly improves agreement with CCSD(T) or experiment (Supporting Information Table S4 and Figures S14-S16). The exception, $X\ ^1\Sigma_g^+$ NiO_2, has a shallow PBE PEC with a bent structure (∠(O-Ni-O) = 168°) nearly degenerate with the linear structure, and increasing HF exchange weakly favors the bent minimum (a_{HF} = 0.4: ∠(O-Ni-O) = 150°, ΔE(linear-bent) = 0.06 eV), an effect that is preserved in fully relaxed structures (Supporting Information Tables S4-S6 and Figure S16).

Focusing on FeO_2 as a representative case, we observe that reduced anti-bonding occupations in the minority spin of $^5B_2$ leads to a significantly deeper PBE PEC (i.e., larger ΔE(linear-bent)) than for the $X\ ^3B_1$ or $^1A_1$ states (Figure 5). The shift in equilibrium ∠(O-Fe-O) with increasing a_{HF} is most significant for the shallower singlet and triplet PECs, but in all cases HF exchange significantly reduces the depth of the PEC (Figure 5). A comparison to the CCSD(T) PECs indicates that moderately high a_{HF} (0.3-0.4) would recover agreement between DFT and the CCSD(T) references for the triplet and quintet states (Figure 5). Conversely, the already linear-favoring PBE PEC for the singlet state is not significantly improved by increasing

a_{HF} (Figure 5). Similar observations hold in comparisons of the steeper high-spin or intermediate-spin MnO_2 and CoO_2 states to their shallower, low-spin counterparts (see Figure 3 and Supporting Information Figures S8 and S15). For CrO_2, this trend reverses due to lower nominal *d* filling, with a more acute, deeper $^1A_1$ PEC also being more sensitive to exchange than the $X\,^3B_1$ state (Supporting Information Figure S14).

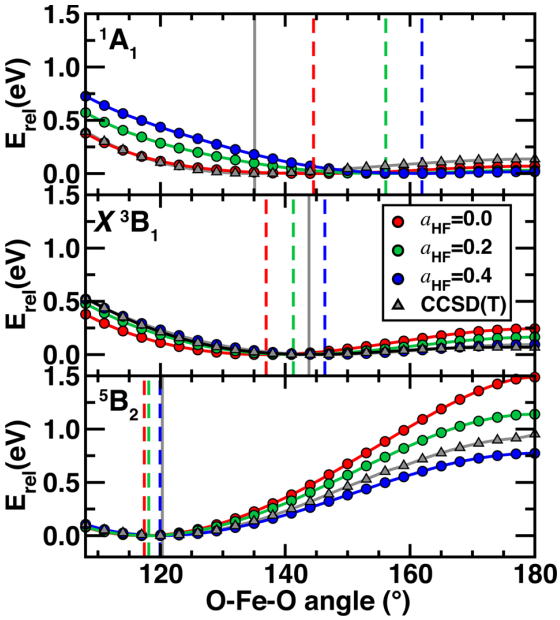

Figure 5. Angular PECs for a fixed $d_{Fe\text{-}O}$=1.58 Å in the low-lying states of FeO_2 (top: $^1A_1$, middle: $X\,^3B_1$, and bottom: $^5B_2$) computed for PBE at three a_{HF} values: 0.0 (red circles), 0.2 (green circles), and 0.4 (blue circles) as well as CCSD(T) reference (grey triangles). The mnimum energy angle for each PEC is labeled by a vertical line (dashed for DFT, solid for CCSD(T)) of the same color.

To compare underlying factors that determine how the remaining 12 PECs evolve with HF exchange, we compute linearized sensitivities (see Sec. 2) of ∠(O-M-O) and Δ*E*(linear-bent) values for the fixed $d_{M\text{-}O}$ PECs across all MO_2 molecules. The linear approximation holds best ($R^2 \geq 0.95$) for M = Cr, Mn, or Fe but reasonably well in the remaining cases (Supporting Information Tables S4 and S6). A wide range of angular sensitivities is observed both across all states (6-132°/HFX) and the five ground states (15 to 39°/HFX, Supporting Information Table S4). Increasing a_{HF} softens these 12 PECs overall, as evidenced through Δ*E*(linear-bent) values

reduced to roughly half their PBE values for a_{HF} = 0.4, broadly improving agreement with CCSD(T) (Supporting Information Table S6). These changes correspond to a wide range of ΔE(linear-bent) sensitivities for both ground states (-0.08 to -0.80 eV/HFX) and overall (-0.08 to -2.13 eV/HFX, Supporting Information Table S6). Within a single metal or spin state, correlations exist between sensitivities and PBE properties, but no correlation holds across the entire series (Supporting Information Figure S17).

These linearized exchange sensitivities also enable interpolation of an a_{HF} that optimally matches the CCSD(T) ∠(O-M-O) and ΔE(linear-bent) values (Supporting Information Figure S18). For both CrO_2 states, a single optimal a_{HF} (0.1–0.2) improves both well depth and minimum simultaneously, whereas the PECs for singlet states of FeO_2 and NiO_2 cannot be improved with HF exchange (Supporting Information Figure S18). Moderate exchange at higher values (i.e., a_{HF} = 0.2–0.4) than was needed for CrO_2 can generally improve both properties simultaneously for the other states of MnO_2, FeO_2, or NiO_2 (Supporting Information Figure S18). Thus, as judged through these two properties, tuning HF exchange qualitatively improves agreement of DFT PECs with CCSD(T) references. To improve DFT minimum ∠(O-M-O) agreement with CCSD(T) references globally across all molecules and spin states, a relatively low HF exchange fraction (a_{HF} = 0.1-0.2, mean absolute error, MAE = 7°) provides the best compromise (Supporting Information Figure S19). The global improvement over pure PBE (MAE = 8°) is modest due to the strong metal and spin-state dependence of the optimal a_{HF} value (Supporting Information Figure S19).

To determine if these energetic changes are broadly consistent with the effect of hybrid tuning on the density, we compute partial charges of all five ground state MO_2 molecules with both tuned DFT and CCSD(T) methods in their CCSD(T) equilibrium structures (Supporting

Information Figures S2-S6 and S9). As with MnO_2, PBE partial charges are a consistent underestimate of CCSD(T) values, and increasing a_{HF} improves agreement with CCSD(T) (Supporting Information Figure S9). However, the high a_{HF} values around 0.4 that are needed to recover the best agreement with CCSD(T) are higher than the values that improve agreement for PEC characteristics in some cases (e.g., CrO_2, Supporting Information Figure S9). Overall, hybrid tuning improves density and energy properties synergistically but not at a one-size-fits-all a_{HF} value.

To further rationalize differences in exchange sensitivity across metals and spin states, we compare averaged density properties of the δ molecular orbital (MO) with metal d_{x2-y2} character, since the excess delocalization of density into the non-bonded O···O interaction was observed to be key to explaining effects of hybrid tuning on $X\,^4B_1$ MnO_2. We integrate the total doubly-occupied (i.e., spin-up and -down $\rho(\delta(d_{x2-y2}))=|\phi_\alpha|^2+|\phi_\beta|^2$) PBE density in the *x*- and *y*-directions after orienting the molecule with the O···O vector along the z-axis (see Figure 6 inset):

$$\rho(z) = \int_{-\infty}^{\infty} \rho(\vec{r})\,dx\,dy \tag{2}$$

We first analyze the densities in the ground state $X\,^3B_1$ and low-lying $^1A_1$ or $^5B_2$ states of FeO_2, which were noted to have distinct structural sensitivities to HF exchange, to ascertain whether characteristics of the $\delta(d_{x2-y2})$ density might underlie these differences. Distinct $\rho(z)$ profiles are observed at a single fixed geometry (d(Fe-O) = 1.58 Å, ∠(O-Fe-O) = 144°) for the three spin states, with predominant localization on the metal (z = 0) for $^5B_2$ FeO_2 and more distributed metal- and oxygen-centered densities in $X\,^3B_1$ or $^1A_1$ FeO_2 (Figure 6). The triplet and singlet states differ most in the broader peak widths for the triplet; the relative metal and oxygen peak heights are comparable in the singlet, whereas the triplet has enhanced metal density

(Figure 6). These differences in $\rho(z)$ for the $\delta(d_{x2-y2})$ orbital are associated with differences in HF exchange sensitivity: the least delocalization in the $^5B_2$ $\delta(d_{x2-y2})$ density correlates to the lowest geometric (i.e., ∠(O-Fe-O)) sensitivity (Figure 6).

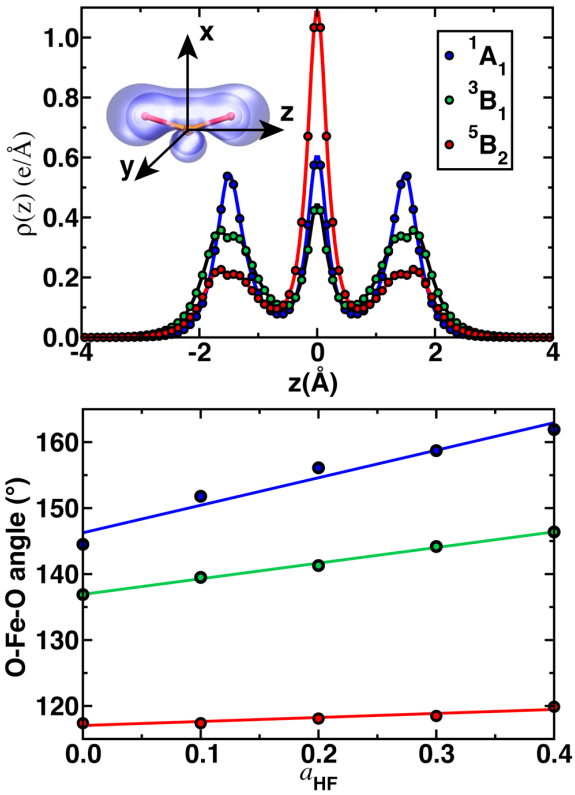

Figure 6. (top) Distribution of total spin-up and spin-down $\delta(d_{x2-y2})$ PBE-calculated electron density averaged along the z-axis, $\rho(z)$ (in e/Å), for three low-lying states of FeO_2: $^1A_1$, *X* $^3B_1$, and $^5B_2$. The same FeO_2 structure (bond length: 1.58 Å, ∠(O-Fe-O): 144°) is used for comparison of the electron density of the three spin states, and the alignment of the molecule to the *z*-axis is depicted in inset. (bottom) Optimized ∠(O-Fe-O) (in °) from the PEC (d_{Fe-O} =1.58 Å) for the three low-lying states of FeO_2 with increasing a_{HF} from 0.0 to 0.4 along with linear fits colored according to the legend in the top pane.

We repeat the analysis for the averaged, total density of the doubly-occupied, nominally bonding (i.e., $\sigma(d_{z2})$, $\pi(d_{xz})$, $\pi(d_{yz})$) and non-bonding (i.e., $\delta(d_{xy})$) MOs with 3*d* character for all three FeO_2 states. The bonding states are equivalently delocalized regardless of spin state, whereas $\delta(d_{xy})$ trends are the same as for $\delta(d_{x2-y2})$, motivating a focus on the δ-derived density (Supporting Information Figure S20). Extension of this analysis to other MO_2 molecules shows

balanced, broad peak heights for CrO_2 that are comparable for both singlet and triplet states and also have high angular sensitivities similar to the most sensitive (i.e., singlet) FeO_2 state (Supporting Information Figure S21). For MnO_2, a more FeO_2-like spin-state dependence of delocalization and exchange sensitivities is observed; the more delocalized doublet has greater sensitivity than the quartet (Supporting Information Figure S22).

Although this analysis has been focused on PBE MO densities, the density can be expected to evolve with increasing a_{HF} (see Figure 3). Increasing HF exchange fraction has almost no effect on the already metal-localized $^5B_2$ $\rho(z)$ for the $\delta(d_{x2-y2})$ MO in FeO_2, whereas significant changes occur for the $^1A_1$ and $X\ ^3B_1$ $\rho(z)$, localizing density away from or onto the metal, respectively (Supporting Information Figure S23). Thus, enhanced geometric sensitivity of low-spin states over high-spin states can be interpreted in terms of the greater sensitivity of key MO density distributions to HF exchange.

3b. Spin State Energetics for MO_2 molecules.

We have shown that incorporating HF exchange generally improves density and geometry simultaneously within an electronic state, and we expect hybrid tuning to also have a significant effect on energetic ordering of spin states.[20-24, 29, 59, 76] Thus, we next consider whether agreement with experimental ground state assignments for MO_2 molecules are achieved with hybrids as well. We compare low-spin (LS) states (i.e., $^1A_1$ for CrO_2 and FeO_2, $^2B_1$ for MnO_2, $X\ ^2\Delta_g$ for CoO_2 and $X^1\Sigma_g^+$ for NiO_2) to intermediate-spin (IS) states that have two more unpaired electrons (i.e., $X\ ^3B_1$ for CrO_2 and FeO_2, $X\ ^4B_1$ for MnO2, $^4A_1$ for CoO_2, and $^3A_2$ for NiO_2). This qualitative state assignment keeps the change in number of paired electrons consistent, simplifying interpretation of functional sensitivity[24, 29], and we also compare remaining high-spin (HS) states ($^5B_2$ for FeO_2, $^6A_1$ for CoO_2, and $^5A_1$ for NiO_2) in select cases.

The IS states are the experimentally determined ground states for early- to mid-row MO_2 molecules, whereas LS states are preferred for CoO_2 and NiO_2, with HS states always disfavored. To compute spin state energetics, we re-optimize geometries with increasing HF exchange in each spin state (Supporting Information Table S5). Surprisingly given the significant density and geometry errors obtained with PBE, the PBE functional predicts the correct ground state across all five transition metal dioxides (Figure 7). As expected[20-24, 29, 59, 76], IS and HS states are monotonically stabilized with respect to LS states when the HF exchange fraction is increased (Figure 7). Incorporating HF exchange therefore preserves agreement with experimental assignment when IS states are the experimental ground state (Cr, Mn) but worsens agreement for LS ground state transition metal dioxides (Ni or Co) even at modest a_{HF} values (0.1-0.2, Figure 7 and Supporting Information Table S9). For Fe, the IS state remains stabilized with respect to the LS state, but at the high HF exchange values needed to improve $X\,^3B_1$ FeO_2 structural agreement with experiment[89-90] ($\angle$(O-M-O) = 149° at a_{HF} = 0.4 vs. 150° from expt.), the HS state is predicted to be the most stable by 8 kcal/mol (Figure 7 and Supporting Information Tables S5 and S9).

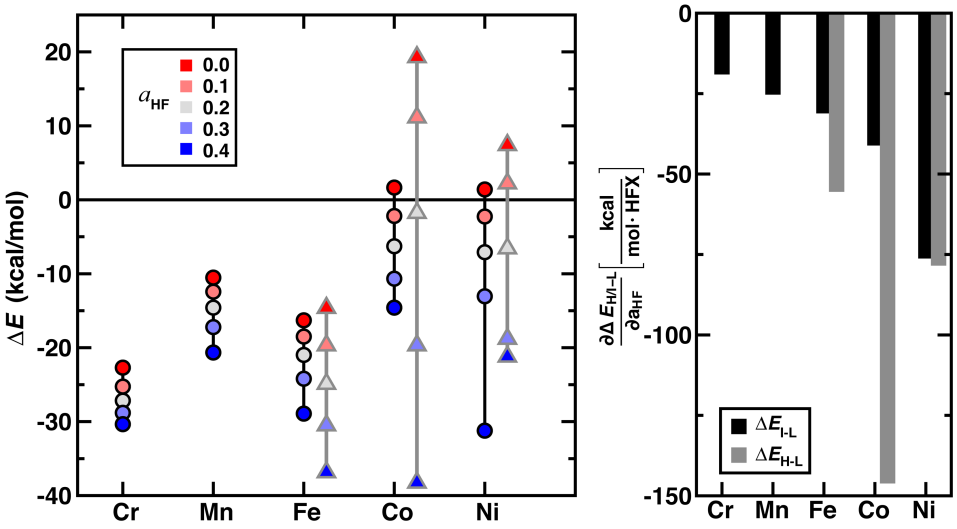

Figure 7. (left) Adiabatic spin-splitting energies (in kcal/mol) for $\Delta E_{I\text{-}L}$ (circles, black lines) and, where applicable, $\Delta E_{H\text{-}L}$ (triangles, gray lines) for MO_2 (M = Cr, Mn, Fe, Co, or Ni). The PBE

results are calculated on fully relaxed geometries for a_{HF} values ranging from 0.0 (red symbols) to 0.4 (blue symbols), as indicated in inset legend. (right) The sensitivity of spin-state energetics with respect to HF exchange (i.e., $\partial\Delta E_{H/I\text{-}L}/\partial a_{HF}$, in kcal/mol·HFX) for the systems studied on the left following the same color scheme (I-L in black and H-L in gray).

To assess the effect of HF exchange on spin-state ordering across these transition metal dioxides, we compare the approximate, linearized exchange sensitivity[22, 24, 29, 54] (see Sec. 2) of the HS/IS to LS adiabatic energy difference (i.e., $\Delta E_{H\text{-}L}$ or $\Delta E_{I\text{-}L}$, Supporting Information Table S9). Across the five molecules studied, increasing 3*d* filling correlates to increasing $\Delta E_{I\text{-}L}$ exchange sensitivity, in contrast with other properties (e.g., ΔE(linear-bent)) that showed no such 3*d* filling dependence (Figure 7 and Supporting Information Tables S6 and S9). Delocalization differences between the states being compared[54, 129] (e.g., IS and LS in spin-splitting energies[54]) have been proposed to correlate to exchange sensitivities. To quantify differences in relative delocalization across the transition metal dioxides, we again compare the $\rho(z)$ of $\delta(d_{x2\text{-}y2})$ states (see Sec. 3a). Integrating the area under the metal-centered peak of the density (i.e., between the $\rho(z)$ local minima) reveals an increasing amount of metal-localized density for the IS states but decreased metal-localized density in the LS states with increasing 3*d* filling (Supporting Information Figure S24). Increasing exchange sensitivity magnitudes demonstrate a good linear correlation (R^2=0.91) to the increasing imbalances in delocalization between the LS and IS states (Supporting Information Figure S24). For Fe, Co, and Ni, $\Delta E_{H\text{-}L}$ sensitivities are higher than the equivalent $\Delta E_{I\text{-}L}$ values, but no monotonic trend is observed (Figure 7).

We also consider whether differences in the effect of HF exchange on geometries (i.e., $d_{M\text{-}O}$ and ∠(O-M-O)) for each spin state might influence the differing spin-state-ordering exchange sensitivities. The PBE M-O bonds agree within 0.01–0.03 Å for IS and LS states, being slightly shorter in the LS state (Supporting Information Table S5). Incorporating HF

exchange causes all LS state M-O bonds to shorten by 0.01–0.05 Å, whereas the effect on the IS state is more variable, leading to greater differences in IS and LS $d_{M\text{-}O}$ at high a_{HF} values especially for later transition metal FeO_2 and NiO_2 but not CoO_2 (Supporting Information Table S5). Thus, geometric changes compound spin-state sensitivity in cases with M-O bond elongation (e.g., $^5A_1$ and $^3A_2$ NiO_2 or $^6A_1$ CoO_2) corresponding to a bent-to-linear transition at high HF exchange values, although this observation does not explain all high-sensitivity cases (e.g., for the ∠(O-Fe-O) = 120° $^5B_2$ FeO_2 case, Supporting Information Table S5).

Overall, these observations indicate that single-parameter tuning of a global hybrid can improve density and geometry in a consistent manner but cannot be anticipated to simultaneously recover spin-state energetics. The significant multi-reference character of nearly all states considered could point toward static correlation error playing an overriding role in relative spin-state energetics at high fractions of HF exchange (Supporting Information Table S3).

3c. Energetic Trends in Diatomic Species.

To determine how broadly applicable our observations on transition metal dioxides are to metal–organic bonds, we evaluate the effect of method choice on densities and structures in related transition metal diatomics. We examine five previously-studied[130] isoelectronic diatomics that are nominally expected to have more ionic (i.e., CrF, CrO^-) or more covalent (i.e., MnO, FeN, and FeO^+) character. For consistency, we study only a single $^6\Sigma^+$ electronic state, which is the known experimental ground state in most cases[88, 96-103]. From the PECs of these molecules evaluated with DFT or CCSD(T), we extract equilibrium bond lengths (r_e), harmonic frequencies (ω_e), and bond dissociation energies (D_e) (Table 1 and Supporting Information Tables S2 and S10).

Table 1. Comparison of calculated properties for $^6\Sigma^+$ isoelectronic diatomics: bond lengths (r_e, in Å), harmonic frequencies (ω_e, in cm^{-1}), and dissociation energies (D_e, in eV). Results are obtained for PBE with a_{HF} = 0.0 to 0.4 in increments of 0.1 as well as a CCSD(T) reference and compared to available experimental results (Expt.).

		a_{HF}					CCSD(T)	Expt.
		0.0	0.1	0.2	0.3	0.4		
CrF	r_e	1.788	1.788	1.786	1.786	1.784	1.784	1.784[a]
	ω_e	647	648	651	653	657	676	664[a]
	D_e	5.23	5.08	4.94	4.82	4.72	4.69	4.57[b]
CrO^-	r_e	1.680	1.678	1.678	1.678	1.676	1.688	--
	ω_e	836	841	845	850	855	845	780±80[c]
	D_e	4.57	4.24	3.95	3.68	3.44	4.00	--
MnO	r_e	1.625	1.621	1.622	1.629	1.643	1.639	1.648[d]
	ω_e	913	912	893	851	773	839	833[d]
	D_e	5.26	4.71	4.20	3.76	3.40	3.28	3.83[e]
FeN[d]	r_e	1.610	1.604	1.604	1.614	1.628	1.595	--
	ω_e	898	880	832	767	723	912	--
	D_e	3.37	3.05	2.60	2.18	1.82	2.92	--
FeO^+	r_e	1.632	1.626	1.622	1.622	1.628	1.640	1.643[f], 1.641[g]
	ω_e	868	873	863	836	802	706	844[g]
	D_e	4.62	4.01	3.43	2.91	2.42	3.19	3.52±0.02[h]

a. Fourier transform spectrophotometry, reference[96-97]
b. Thermochemical value (mass-spectrum), reference[131]
c. Ultraviolet negative-ion photoelectron spectroscopy, reference[98]
d. Electronic spectroscopy, reference[99-100]
e. Photoelectron spectroscopy, reference[88]
f. Resonance enhanced photodissociation spectroscopy, reference[101]
g. Microwave spectroscopy, reference[102]
h. Photoionization efficiency curve, reference[103]

Consistent with expected ionic or covalent character, CrF and CrO^- have longer PBE r_e values of 1.79 Å and 1.68 Å in comparison to a shorter r_e around 1.61-1.63 for FeN, MnO, and FeO^+ (Table 1). As for the MO_2 cases, incorporating HF exchange has a limited impact on equilibrium bond length (CrF or CrO^-: 0.004 Å, MnO, FeN, and FeO^+: 0.02-0.03 Å from a_{HF}=0.0 to 0.4) in these systems, unlike observations[130] with DFT+U (Table 1). The PBE bond lengths of

all five diatomic molecules are generally within 0.01-0.02 Å of the CCSD(T) values or experiment, and the modest effect of exchange on structure means a_{HF} cannot be tuned to improve this agreement (Table 1).

As with bond lengths, HF exchange has a divergent effect on harmonic frequencies, ω_e, of the covalent and ionic diatomics (Figure 8). Incorporating HF exchange lowers the frequencies of the covalent MnO, FeN, or FeO^+ by around 70 to 180 cm^{-1}, whereas the frequencies of CrF and CrO^- are increased slightly by 10–20 cm^{-1}. This reduction in ω_e of the covalent cases is consistent with the softening of the PEC we observed in MnO_2 or FeO_2, whereas the behavior of the ionic CrF and CrO^- species differs slightly from our previous observations (Figure 8). Incorporating exchange improves agreement of DFT-calculated ω_e values with CCSD(T) for four of the five cases, significantly improving the most delocalized, covalent cases of FeO^+ and MnO and slightly improving CrF and CrO^- (Figure 8). Analysis of these four diatomics would motivate an a_{HF} = 0.4, but a very high CCSD(T) frequency in FeN cannot be reproduced at non-zero values of a_{HF}. This analysis highlights the limitations of HF exchange tuning for correcting all imbalances in the DFT treatment of the metal–organic bond.

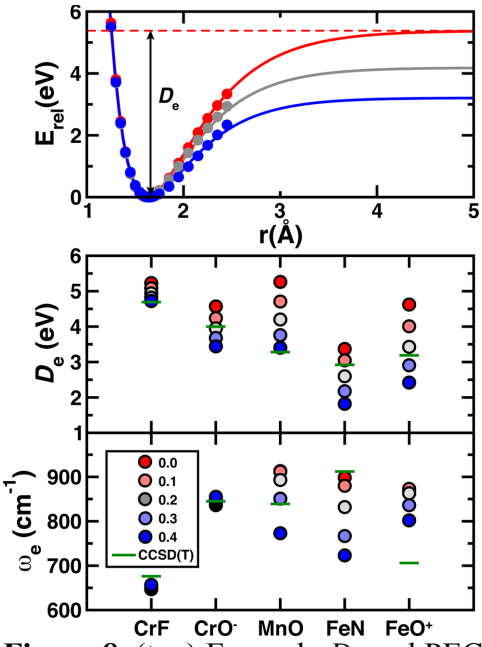

Figure 8. (top) Example D_e and PECs for $^6\Sigma^+$ MnO evaluated at a_{HF} = 0.0 (red lines and circles), 0.2 (gray lines and circles), and 0.4 (blue lines and circles) with a Morse potential fit through each data set shown, and the PBE D_e annotated as a red dashed line. (bottom) D_e (middle pane) and ω_e (bottom pane) of $^6\Sigma^+$ isoelectronic diatomics with varying a_{HF} values ranging from 0.0 (red symbols) to 0.4 (blue symbols), as indicated in inset legend. The CCSD(T) reference results are shown as green horizontal lines.

All PBE D_e values are significant overestimates of CCSD(T) or experimental values, where available, with the largest overestimates for the more covalent diatomics (Figure 8 and Table 1). Unlike more molecule-specific trends observed for r_e or ω_e, the dissociation energy, D_e, consistently decreases with a_{HF} fraction across all five diatomics (Figure 8). Overall, the D_e decreases linearly with a_{HF} (R^2 = 0.99), with higher sensitivities observed for the more covalent species (Figure 8 and Supporting Information Figure S25). As a result, moderate (a_{HF}=0.2) exchange fractions produce very good agreement with CCSD(T) D_e values in most cases (Figure 8). Higher exchange fractions, which had been motivated for other properties or molecules, would lead to significant underestimation of D_e values in some cases (FeN, FeO^+, and CrO^-) but good agreement in others (CrF and MnO). Overall, the covalent species behave in the expected manner consistent with our observations on the MO_2 series, with lower ω_e, slightly elongated r_e,

and reduced D_e with HF exchange incorporation due to PEC softening. In contrast, the more ionic CrF or CrO^- behave more unexpectedly, where weak increases in ω_e and a shortening of r_e contrast with a reduction in D_e, meriting further investigation of the relationship of these energetic changes to changes in the density.

3d. Density Trends in Diatomic Species.

To analyze the effect of HF exchange on density properties, we again compute metal partial charges, q_M, obtained from Bader analysis[126-127] and evaluated at a fixed 1.635 Å bond distance (see Sec. 2). As with the MO_2 molecules, all PBE q_M values are significant underestimates of CCSD(T) values (i.e., the bond is less polarized), with the largest (ca. 0.3 e) underestimate for negatively charged CrO^-. Incorporation of HF exchange thus improves agreement with CCSD(T) across all five diatomics by generally increasing q_M by 0.08-0.14 e over PBE values when using a_{HF} = 0.4 (Figure 9). This value of a_{HF} coincides with the optimal one for recovering the CCSD(T) value of ω_e but would lead to underestimation of D_e.

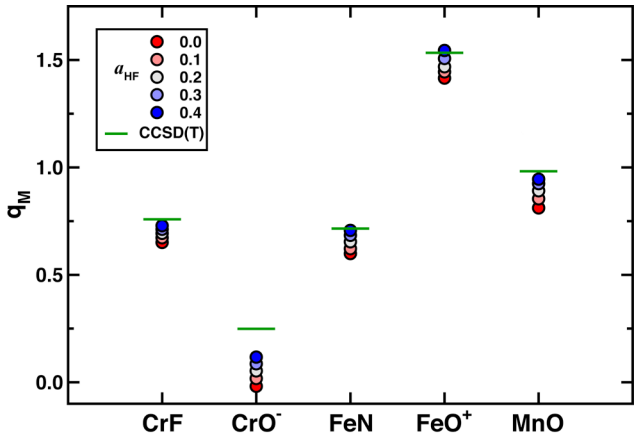

Figure 9. Metal partial charge, q_M, (in e) for $^6\Sigma^+$ diatomic molecules (bond distance: 1.635 Å) calculated using PBE with a_{HF} values ranging from 0.0 to 0.4 (red to blue circles, as in inset legend) and compared to CCSD(T) reference (green lines).

As we did for other quantities, we approximate the sensitivity of the partial charges to HF exchange as a linear quantity (i.e., $\partial q_M/\partial a_{HF} \approx \Delta q_M/\Delta a_{HF}$). The highly ionic species, CrF,

displays the lowest sensitivity of 0.2 e/HFX, whereas all other diatomics are significantly higher (ca. 0.3 e/HFX, Supporting Information Table S11). For a pair of neutral and charged molecules with the same metal atom, the charged molecule exhibits higher sensitivity (e.g., 0.19 e/HFX for CrF vs. 0.34 e/HFX for CrO^-).

To understand the origins of relative sensitivities of structural and partial charge properties across the $^6\Sigma^+$ isoelectronic diatomics, we analyze differences in the electron density following a comparable procedure to that for the MO_2 molecules. The frontier orbitals of the $^6\Sigma^+$ isoelectronic diatomics consist of doubly occupied σ bonding ($3d_{z^2} + 2p_z$) and two π bonding orbitals (π_{xz}: $3d_{xz} + 2p_x$ and π_{yz}: $3d_{yz} + 2p_y$) along with the three corresponding singly-occupied (i.e., spin up σ*, π_{xz}*, and π_{yz}*) anti-bonding orbitals and two singly-occupied metal 3*d* non-bonding (i.e., δ) orbitals (Supporting Information Figure S26). Since differences in the bonding or non-bonding orbitals among the isoelectronic species as well as changes in their character with HF exchange are expected to have the most significant effect on the PECs, we focus on the principal-axis (i.e., *z*) averaged, total spin-up and spin-down PBE density for the bonding orbitals. We align the molecule along the *z*-axis and average the density following eqn. (2) at a fixed 1.635 Å bond distance to facilitate comparison.

In agreement with qualitative expectations of differences in ionic or covalent bond character, the five molecules exhibit distinct density profiles, $\rho(z)$, for both the σ and π bonding orbitals (Figure 10). For all bonding orbitals, the ionic (i.e., CrF and CrO^-) cases exhibit less density in the region between the two nuclei, whereas the more covalent (i.e., FeN, FeO^+, and MnO) cases have a larger fraction of the density in this region (Figure 10). Nominally, charged species have more delocalization of the density in the bond (i.e., are more covalent) than the equivalent (i.e., same metal) neutral species. These trends can be quantified using the standard

deviation of the distribution of $\rho(z)$ values between the nuclei, which we refer to as the fluctuation of the density (see Sec. 2 and Supporting Information Table S12). Smaller fluctuations in the bonding orbitals correspond to more delocalization, e.g. in CrO^- vs. CrF (σ: 0.14 vs. 0.22 e/Å and π_{xz}/π_{yz}: 0.29 vs. 0.44 e/Å), consistent with our earlier observations on differences in these two molecules. For the π_{xz}/π_{yz} orbitals, CrF and CrO^- fluctuations are ca. twice the values (0.16–0.19 e/Å) for the other three molecules, explaining the reduced relative sensitivity of CrF and CrO^- structural properties to HF exchange.

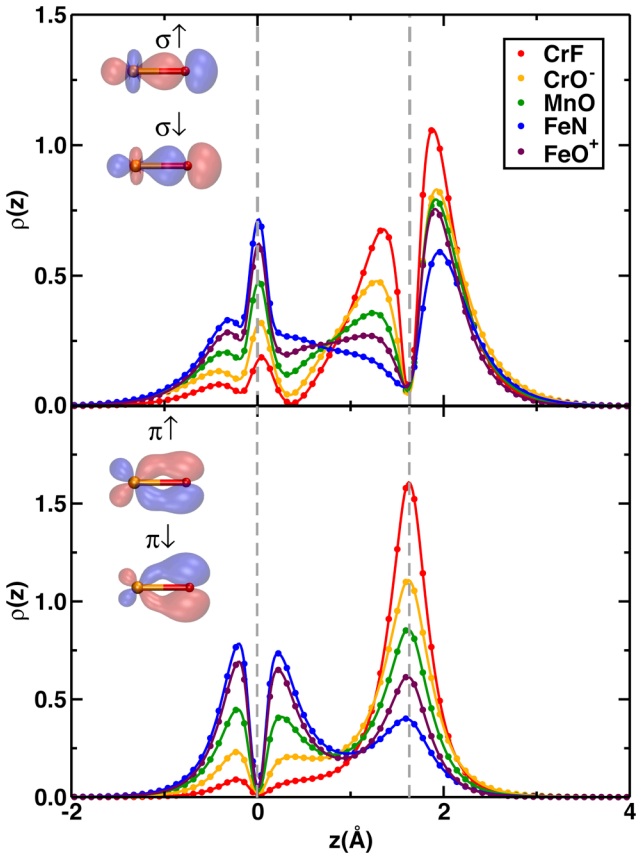

Figure 10. Distribution of total spin-up and spin-down PBE-calculated electron density averaged along the z-axis, $\rho(z)$ (in e/Å), for σ (top) or $\pi_{xz/yz}$ (bottom) bonding orbitals in isoelectronic $^6\Sigma^+$ molecules (bond distance: 1.635 Å). Representative molecular orbitals for MnO are shown in insets (isosurface: 0.1 e/bohr^3). Vertical dashed grey lines indicate the position of the metal (at 0 Å) and the coordinating atom (at 1.635 Å).

For MO_2 molecules, the shapes of highly delocalized orbitals were more sensitive to

hybrid tuning than localized orbitals, a trend that also holds for the $^6\Sigma^+$ diatomics. By evaluating the change in the density distribution, $\Delta\rho(z)$, with increasing a_{HF}, we observe that the more covalent MnO bonding orbitals change more significantly than those of the more ionic CrF (Supporting Information Figure S27).

Apparently at odds with q_M analysis, the $\Delta\rho(z)$ for the MnO bonding orbitals indicates that the density on the metal in these orbitals increases with a_{HF} (see Figure 9 and Supporting Information Figure S27). However, as a_{HF} increases, metal electron density gain in the bonding orbitals (e.g., +0.22 e for Mn in MnO) is offset by depletion in anti-bonding orbitals (e.g., -0.29 e for Mn in MnO) and unaffected by limited changes in the non-bonding orbitals (Supporting Information Figures S28-S29). In comparison to MnO, changes in CrF orbitals of all types are in the same direction but much smaller in magnitude, explaining the lower partial charge sensitivity of more ionic species as well. Overall, HF exchange has a consistent effect on density properties of the $^6\Sigma^+$ states, localizing density away from the bond and therefore in most cases softening potential energy curves, in improved agreement with accurate reference results. However, no single a_{HF} value is likely to work across all types of chemical bonding or all properties.

4. Conclusions.

Using a series of representative transition metal-containing small molecules, we have studied the relationships of semi-local, approximate DFT density, structural, and energetic errors. By comparing to accurate correlated wavefunction theory and experimental references, we have shown how reducing density delocalization error in transition metal triatomics (MO_2, where M = Cr, Mn, Fe, Co, or Ni) through incorporating of HF exchange in most cases also improves the properties of the Born–Oppenheimer potential energy surface (PES) with respect to accurate references. Where semi-local DFT MO_2 angles were too acute and bent structures were too

stabilized, hybrid functionals (a_{HF} = 0.2–0.4) penalized density delocalization in nominally non-bonded δ-type orbitals to produce improved, shallower angular potential energy curves, as evidenced through increased O-M-O angles and reduced ΔE(linear-bent) values or harmonic frequencies. This reduction in density delocalization error could also be observed through increased partial charges on the metal ion, indicative of localization of density onto the oxygen and away from the metal-oxygen bond in improved agreement with CCSD(T) partial charges. Evaluation of energetic and density properties of a series of isoelectronic $^6\Sigma^+$ diatomic molecules indicated that these observations on triatomics were general to covalent metal–organic bonds (e.g., in MnO, FeO^+, and FeN) but divergent from the behavior of more ionic bonds (e.g., in CrO^- and CrF).

Although the optimal choice of exchange was seen to be both property and system specific, incorporating HF exchange tended to synergistically improve properties of density, structure, and energetics within a single PES characterized by moderately covalent bonding. The same improvement was not be observed in the ordering between MO_2 spin states, as already good agreement of semi-local DFT spin state ordering with CCSD(T) or experiment was worsened by over-stabilization of intermediate- and high-spin states when HF exchange was added. This study provides some evidence that hybrid tuning can synergistically improve DFT properties for the right reason by improving density delocalization errors and geometric errors in a physically consistent manner. More work is needed to improve upon this result, including through flexible functional forms that simultaneously correct static correlation error and delocalization error.

ASSOCIATED CONTENT

Supporting Information. Details of frequency analysis; dissociating species identities; basis set convergence tests; 2D PESes from CCSD(T); Bader charge convergence tests; multi-reference diagnostics of triatomics and diatomics; energetics of bent vs. linear MO_2 structures; angle and bond of low-lying states of MO_2 molecules; PECs of low-lying states of MnO_2, CrO_2, CoO_2, and NiO_2 molecules; correlations of PEC properties and sensitivities; optimal a_{HF} for well depth and angle; density analysis of FeO_2, CrO_2, and MnO_2 low-lying states; spin state ordering of MO_2 molecules; sensitivity of diatomic properties to HF exchange including dissociation energy and partial charges; standard deviations of charges between nuclei for diatomic molecules; frontier orbital properties and their changes with HF exchange; comparison to range-separated hybrid tuning. (PDF)

AUTHOR INFORMATION

Corresponding Author

*email: hjkulik@mit.edu phone: 617-253-4584

Notes

The authors declare no competing financial interest.

ACKNOWLEDGMENT

This material is based upon work supported by the U.S. Department of Energy, Office of Science, Office of Basic Energy Sciences under Award Number DE-SC0018096. H.J.K. holds a Career Award at the Scientific Interface from the Burroughs Wellcome Fund and an AAAS Marion Milligan Mason Award, which supported this work. The authors thank Adam H. Steeves for providing a critical reading of the manuscript.

References

1. Mori-Sánchez, P.; Cohen, A. J.; Yang, W., Many-Electron Self-Interaction Error in Approximate Density Functionals. *J. Chem. Phys.* **2006,** *125*, 201102.
2. Ruzsinszky, A.; Perdew, J. P.; Csonka, G. I.; Vydrov, O. A.; Scuseria, G. E., Density Functionals That Are One- and Two- Are Not Always Many-Electron Self-Interaction-Free, as Shown for H2+, He2+, LiH+, and Ne2+. *J. Chem. Phys.* **2007,** *126*, 104102.
3. Haunschild, R.; Henderson, T. M.; Jiménez-Hoyos, C. A.; Scuseria, G. E., Many-Electron Self-Interaction and Spin Polarization Errors in Local Hybrid Density Functionals. *J. Chem. Phys.* **2010,** *133*, 134116.
4. Cohen, A. J.; Mori-Sánchez, P.; Yang, W., Insights into Current Limitations of Density Functional Theory. *Science* **2008,** *321*, 792-794.
5. Schmidt, T.; Kümmel, S., One- and Many-Electron Self-Interaction Error in Local and Global Hybrid Functionals. *Phys. Rev. B* **2016,** *93*, 165120.
6. Kim, M.-C.; Sim, E.; Burke, K., Understanding and Reducing Errors in Density Functional Calculations. *Phys. Rev. Lett.* **2013,** *111*, 073003.
7. Zheng, X.; Liu, M.; Johnson, E. R.; Contreras-García, J.; Yang, W., Delocalization Error of Density-Functional Approximations: A Distinct Manifestation in Hydrogen Molecular Chains. *J. Chem. Phys.* **2012,** *137*, 214106.
8. Johnson, E. R.; Otero-de-la-Roza, A.; Dale, S. G., Extreme Density-Driven Delocalization Error for a Model Solvated-Electron System. *J. Chem. Phys.* **2013,** *139*, 184116.
9. Tozer, D. J.; De Proft, F., Computation of the Hardness and the Problem of Negative Electron Affinities in Density Functional Theory. *J. Phys. Chem. A* **2005,** *109*, 8923-8929.
10. Teale, A. M.; De Proft, F.; Tozer, D. J., Orbital Energies and Negative Electron Affinities from Density Functional Theory: Insight from the Integer Discontinuity. *J. Chem. Phys.* **2008,** *129*, 044110.
11. Peach, M. J. G.; Teale, A. M.; Helgaker, T.; Tozer, D. J., Fractional Electron Loss in Approximate DFT and Hartree–Fock Theory. *J. Chem. Theory Comput.* **2015,** *11*, 5262-5268.
12. Mori-Sánchez, P.; Cohen, A. J.; Yang, W., Localization and Delocalization Errors in Density Functional Theory and Implications for Band-Gap Prediction. *Phys. Rev. Lett.* **2008,** *100*, 146401.
13. Cohen, A. J.; Mori-Sánchez, P.; Yang, W., Fractional Charge Perspective on the Band Gap in Density-Functional Theory. *Phys. Rev. B* **2008,** *77*, 115123.
14. Johnson, B. G.; Gonzales, C. A.; Gill, P. M. W.; Pople, J. A., A Density Functional Study of the Simplest Hydrogen Abstraction Reaction. Effect of Self-Interaction Correction. *Chem. Phys. Lett.* **1994,** *221*, 100-108.
15. Ruzsinszky, A.; Perdew, J. P.; Csonka, G. I.; Vydrov, O. A.; Scuseria, G. E., Spurious Fractional Charge on Dissociated Atoms: Pervasive and Resilient Self-Interaction Error of Common Density Functionals. *J. Chem. Phys.* **2006,** *125*, 194112.
16. Dutoi, A. D.; Head-Gordon, M., Self-Interaction Error of Local Density Functionals for Alkali–Halide Dissociation. *Chem. Phys. Lett.* **2006,** *422*, 230-233.
17. Bally, T.; Sastry, G. N., Incorrect Dissociation Behavior of Radical Ions in Density Functional Calculations. *J. Phys. Chem. A* **1997,** *101*, 7923-7925.
18. Zhang, Y.; Yang, W., A Challenge for Density Functionals: Self-Interaction Error Increases for Systems with a Noninteger Number of Electrons. *J. Chem. Phys.* **1998,** *109*, 2604-2608.

19. Kulik, H. J.; Cococcioni, M.; Scherlis, D. A.; Marzari, N., Density Functional Theory in Transition-Metal Chemistry: A Self-Consistent Hubbard U Approach. *Phys. Rev. Lett.* **2006,** *97*, 103001.
20. Ganzenmüller, G.; Berkaïne, N.; Fouqueau, A.; Casida, M. E.; Reiher, M., Comparison of Density Functionals for Differences between the High- (T2g5) and Low- (A1g1) Spin States of Iron(II) Compounds. IV. Results for the Ferrous Complexes [Fe(L)('NHS4')]. *J. Chem. Phys.* **2005,** *122*, 234321.
21. Droghetti, A.; Alfè, D.; Sanvito, S., Assessment of Density Functional Theory for Iron (II) Molecules across the Spin-Crossover Transition. *J. Chem. Phys.* **2012,** *137*, 124303.
22. Ioannidis, E. I.; Kulik, H. J., Towards Quantifying the Role of Exact Exchange in Predictions of Transition Metal Complex Properties. *J. Chem. Phys.* **2015,** *143*, 034104.
23. Mortensen, S. R.; Kepp, K. P., Spin Propensities of Octahedral Complexes from Density Functional Theory. *J. Phys. Chem. A* **2015,** *119*, 4041-4050.
24. Ioannidis, E. I.; Kulik, H. J., Ligand-Field-Dependent Behavior of Meta-GGA Exchange in Transition-Metal Complex Spin-State Ordering. *J. Phys. Chem. A* **2017,** *121*, 874-884.
25. Da Silva, J. L.; Ganduglia-Pirovano, M. V.; Sauer, J.; Bayer, V.; Kresse, G., Hybrid Functionals Applied to Rare-Earth Oxides: The Example of Ceria. *Phys. Rev. B* **2007,** *75*, 045121.
26. Ping, Y.; Galli, G.; Goddard III, W. A., Electronic Structure of IrO2: The Role of the Metal d Orbitals. *J. Phys. Chem. C* **2015,** *119*, 11570-11577.
27. He, J.; Chen, M.-X.; Chen, X.-Q.; Franchini, C., Structural Transitions and Transport-Half-Metallic Ferromagnetism in Lamno 3 at Elevated Pressure. *Phys. Rev. B* **2012,** *85*, 195135.
28. Wilbraham, L.; Adamo, C.; Ciofini, I., Communication: Evaluating Non-Empirical Double Hybrid Functionals for Spin-State Energetics in Transition-Metal Complexes. *J. Chem. Phys.* **2018,** *148*, 041103.
29. Liu, F.; Yang, T.; Yang, J.; Xu, E.; Bajaj, A.; Kulik, H. J., Bridging the Homogeneous-Heterogeneous Divide: Modeling Spin and Reactivity in Single Atom Catalysis. *Front. Chem.* **2019,** *7*, 219.
30. Bao, J. L.; Gagliardi, L.; Truhlar, D. G., Self-Interaction Error in Density Functional Theory: An Appraisal. *J. Phys. Chem. Lett.* **2018,** *9*, 2353-2358.
31. Janesko, B. G., Reducing Density-Driven Error without Exact Exchange. *Phys. Chem. Chem. Phys.* **2017,** *19*, 4793-4801.
32. Wilbraham, L.; Verma, P.; Truhlar, D. G.; Gagliardi, L.; Ciofini, I., Multiconfiguration Pair-Density Functional Theory Predicts Spin-State Ordering in Iron Complexes with the Same Accuracy as Complete Active Space Second-Order Perturbation Theory at a Significantly Reduced Computational Cost. *J. Phys. Chem. Lett.* **2017,** *8*, 2026-2030.
33. Waitt, C.; Ferrara, N. M.; Eshuis, H., Thermochemistry and Geometries for Transition-Metal Chemistry from the Random Phase Approximation. *J. Chem. Theory Comput.* **2016,** *12*, 5350-5360.
34. Kulik, H. J., Perspective: Treating Electron over-Delocalization with the DFT+U Method. *J. Chem. Phys.* **2015,** *142*, 240901.
35. Anisimov, V. I.; Zaanen, J.; Andersen, O. K., Band Theory and Mott Insulators: Hubbard U Instead of Stoner I. *Phys. Rev. B* **1991,** *44*, 943.
36. Liechtenstein, A.; Anisimov, V.; Zaanen, J., Density-Functional Theory and Strong Interactions: Orbital Ordering in Mott-Hubbard Insulators. *Phys. Rev. B* **1995,** *52*, R5467.

37. Stein, T.; Kronik, L.; Baer, R., Prediction of Charge-Transfer Excitations in Coumarin-Based Dyes Using a Range-Separated Functional Tuned from First Principles. *J. Chem. Phys.* **2009,** *131*, 244119.
38. Refaely-Abramson, S.; Baer, R.; Kronik, L., Fundamental and Excitation Gaps in Molecules of Relevance for Organic Photovoltaics from an Optimally Tuned Range-Separated Hybrid Functional. *Phys. Rev. B* **2011,** *84*, 075144.
39. Kronik, L.; Stein, T.; Refaely-Abramson, S.; Baer, R., Excitation Gaps of Finite-Sized Systems from Optimally Tuned Range-Separated Hybrid Functionals. *J. Chem. Theory Comput.* **2012,** *8*, 1515-1531.
40. Gledhill, J. D.; Peach, M. J. G.; Tozer, D. J., Assessment of Tuning Methods for Enforcing Approximate Energy Linearity in Range-Separated Hybrid Functionals. *J. Chem. Theory Comput.* **2013,** *9*, 4414-4420.
41. Karolewski, A.; Kronik, L.; Kümmel, S., Using Optimally Tuned Range Separated Hybrid Functionals in Ground-State Calculations: Consequences and Caveats. *J. Chem. Phys.* **2013,** *138*, 204115.
42. Sun, H.; Autschbach, J., Influence of the Delocalization Error and Applicability of Optimal Functional Tuning in Density Functional Calculations of Nonlinear Optical Properties of Organic Donor–Acceptor Chromophores. *ChemPhysChem* **2013,** *14*, 2450-2461.
43. Autschbach, J.; Srebro, M., Delocalization Error and "Functional Tuning" in Kohn–Sham Calculations of Molecular Properties. *Acc. Chem. Res.* **2014,** *47*, 2592-2602.
44. Körzdörfer, T.; Brédas, J.-L., Organic Electronic Materials: Recent Advances in the DFT Description of the Ground and Excited States Using Tuned Range-Separated Hybrid Functionals. *Acc. Chem. Res.* **2014,** *47*, 3284-3291.
45. Yu, H. S.; Li, S. L.; Truhlar, D. G., Perspective: Kohn-Sham Density Functional Theory Descending a Staircase. *J. Chem. Phys.* **2016,** *145*, 130901.
46. Mardirossian, N.; Head-Gordon, M., ωB97X-V: A 10-Parameter, Range-Separated Hybrid, Generalized Gradient Approximation Density Functional with Nonlocal Correlation, Designed by a Survival-of-the-Fittest Strategy. *Phys. Chem. Chem. Phys.* **2014,** *16*, 9904-9924.
47. Zhao, Q.; Ioannidis, E. I.; Kulik, H. J., Global and Local Curvature in Density Functional Theory. *J. Chem. Phys.* **2016,** *145*, 054109.
48. Mosey, N. J.; Carter, E. A., Ab Initio Evaluation of Coulomb and Exchange Parameters for DFT+ U Calculations. *Phys. Rev. B* **2007,** *76*, 155123.
49. Cococcioni, M.; De Gironcoli, S., Linear Response Approach to the Calculation of the Effective Interaction Parameters in the LDA+ U Method. *Phys. Rev. B* **2005,** *71*, 035105.
50. Stein, T.; Autschbach, J.; Govind, N.; Kronik, L.; Baer, R., Curvature and Frontier Orbital Energies in Density Functional Theory. *J. Phys. Chem. Lett.* **2012,** *3*, 3740-3744.
51. Skone, J. H.; Govoni, M.; Galli, G., Self-Consistent Hybrid Functional for Condensed Systems. *Phys. Rev. B* **2014,** *89*, 195112.
52. Shimazaki, T.; Asai, Y., First Principles Band Structure Calculations Based on Self-Consistent Screened Hartree–Fock Exchange Potential. *J. Chem. Phys.* **2009,** *130*, 164702.
53. Jensen, F., Method Calibration or Data Fitting? *J. Chem. Theory Comput.* **2018,** *14*, 4651-4661.
54. Gani, T. Z. H.; Kulik, H. J., Unifying Exchange Sensitivity in Transition Metal Spin-State Ordering and Catalysis through Bond Valence Metrics *J. Chem. Theory Comput.* **2017,** *13*, 5443-5457.

55. Moltved, K. A.; Kepp, K. P., The Metal Hydride Problem of Computational Chemistry: Origins and Consequences. *J. Phys. Chem. A* **2019,** *123*, 2888-2900.
56. Bowman, D. N.; Jakubikova, E., Low-Spin Versus High-Spin Ground State in Pseudo-Octahedral Iron Complexes. *Inorg. Chem.* **2012,** *51*, 6011-6019.
57. Smith, D. M.; Dupuis, M.; Straatsma, T., Multiplet Splittings and Other Properties from Density Functional Theory: An Assessment in Iron–Porphyrin Systems. *Mol. Phys.* **2005,** *103*, 273-278.
58. Bruschi, M.; De Gioia, L.; Zampella, G.; Reiher, M.; Fantucci, P.; Stein, M., A Theoretical Study of Spin States in Ni-S4 Complexes and Models of the [NiFe] Hydrogenase Active Site. *J. Biol. Inorg. Chem.* **2004,** *9*, 873-884.
59. Verma, P.; Varga, Z.; Klein, J. E.; Cramer, C. J.; Que, L.; Truhlar, D. G., Assessment of Electronic Structure Methods for the Determination of the Ground Spin States of Fe (II), Fe (III) and Fe (IV) Complexes. *Phys. Chem. Chem. Phys.* **2017,** *19*, 13049-13069.
60. Simm, G. N.; Reiher, M., Systematic Error Estimation for Chemical Reaction Energies. *J. Chem. Theory Comput.* **2016,** *12*, 2762-2773.
61. Janesko, B. G.; Proynov, E.; Kong, J.; Scalmani, G.; Frisch, M. J., Practical Density Functionals Beyond the Overdelocalization–Underbinding Zero-Sum Game. *J. Phys. Chem. Lett.* **2017,** *8*, 4314-4318.
62. Bajaj, A.; Janet, J. P.; Kulik, H. J., Communication: Recovering the Flat-Plane Condition in Electronic Structure Theory at Semi-Local DFT Cost. *J. Chem. Phys.* **2017,** *147*, 191101.
63. Bajaj, A.; Liu, F.; Kulik, H. J., Non-Empirical, Low-Cost Recovery of Exact Conditions with Model-Hamiltonian Inspired Expressions in jmDFT. *J. Chem. Phys.* **2019,** *150*, 154115.
64. Modrzejewski, M.; Chalasinski, G.; Szczesniak, M. M., Assessment of Newest Meta-GGA Hybrids for Late Transition Metal Reactivity: Fractional Charge and Fractional Spin Perspective. *J. Phys. Chem. C* **2018,** *123*, 8047-8056.
65. Bochevarov, A. D.; Friesner, R. A., The Densities Produced by the Density Functional Theory: Comparison to Full Configuration Interaction. *J. Chem. Phys.* **2008,** *128*, 034102.
66. He, Y.; Gräfenstein, J.; Kraka, E.; Cremer, D., What Correlation Effects Are Covered by Density Functional Theory? *Mol. Phys.* **2000,** *98*, 1639-1658.
67. Kepp, K. P., Comment on "Density Functional Theory Is Straying from the Path toward the Exact Functional". *Science* **2017,** *356*, 496.
68. Medvedev, M. G.; Bushmarinov, I. S.; Sun, J.; Perdew, J. P.; Lyssenko, K. A., Density Functional Theory Is Straying from the Path toward the Exact Functional. *Science* **2017,** *355*, 49-52.
69. Brorsen, K. R.; Yang, Y.; Pak, M. V.; Hammes-Schiffer, S., Is the Accuracy of Density Functional Theory for Atomization Energies and Densities in Bonding Regions Correlated? *J. Phys. Chem. Lett.* **2017,** *8*, 2076-2081.
70. Mezei, P. D.; Csonka, G. I.; Kállay, M., Electron Density Errors and Density-Driven Exchange-Correlation Energy Errors in Approximate Density Functional Calculations. *J. Chem. Theory Comput.* **2017,** *13*, 4753-4764.
71. Hait, D.; Head-Gordon, M., How Accurate Is Density Functional Theory at Predicting Dipole Moments? An Assessment Using a New Database of 200 Benchmark Values. *J. Chem. Theory Comput.* **2018,** *14*, 1969-1981.
72. Janesko, B. G.; Scuseria, G. E., Hartree–Fock Orbitals Significantly Improve the Reaction Barrier Heights Predicted by Semilocal Density Functionals. *J. Chem. Phys.* **2008,** *128*, 244112.

73. Verma, P.; Perera, A.; Bartlett, R. J., Increasing the Applicability of DFT I: Non-Variational Correlation Corrections from Hartree–Fock DFT for Predicting Transition States. *Chem. Phys. Lett.* **2012,** *524*, 10-15.
74. Kim, M.-C.; Sim, E.; Burke, K., Ions in Solution: Density Corrected Density Functional Theory (DC-DFT). *J. Chem. Phys.* **2014,** *140*, 18A528.
75. Kim, M.-C.; Park, H.; Son, S.; Sim, E.; Burke, K., Improved DFT Potential Energy Surfaces via Improved Densities. *J. Phys. Chem. Lett.* **2015,** *6*, 3802-3807.
76. Gani, T. Z. H.; Kulik, H. J., Where Does the Density Localize? Convergent Behavior for Global Hybrids, Range Separation, and DFT+U *J. Chem. Theory Comput.* **2016,** *12*, 5931-5945.
77. Brumboiu, I. E.; Prokopiou, G.; Kronik, L.; Brena, B., Valence Electronic Structure of Cobalt Phthalocyanine from an Optimally Tuned Range-Separated Hybrid Functional. *J. Chem. Phys.* **2017,** *147*, 044301.
78. Duignan, T. J.; Autschbach, J., Impact of the Kohn–Sham Delocalization Error on the 4f Shell Localization and Population in Lanthanide Complexes. *J. Chem. Theory Comput.* **2016,** *12*, 3109-3121.
79. Duignan, T. J.; Autschbach, J.; Batista, E.; Yang, P., Assessment of Tuned Range Separated Exchange Functionals for Spectroscopies and Properties of Uranium Complexes. *J. Chem. Theory Comput.* **2017,** *13*, 3614-3625.
80. Srebro, M.; Autschbach, J., Does a Molecule-Specific Density Functional Give an Accurate Electron Density? The Challenging Case of the Cucl Electric Field Gradient. *J. Phys. Chem. Lett.* **2012,** *3*, 576-581.
81. Pritchard, B.; Autschbach, J., Theoretical Investigation of Paramagnetic NMR Shifts in Transition Metal Acetylacetonato Complexes: Analysis of Signs, Magnitudes, and the Role of the Covalency of Ligand–Metal Bonding. *Inorg. Chem.* **2012,** *51*, 8340-8351.
82. Song, S.; Kim, M.-C.; Sim, E.; Benali, A.; Heinonen, O.; Burke, K., Benchmarks and Reliable DFT Results for Spin Gaps of Small Ligand Fe (II) Complexes. *J. Chem. Theory Comput.* **2018,** *14*, 2304-2311.
83. Zhao, Q.; Kulik, H. J., Where Does the Density Localize in the Solid State? Divergent Behavior for Hybrids and DFT+U. *J. Chem. Theory Comput.* **2018,** *14*, 670-683.
84. Zhao, Q.; Kulik, H. J., Stable Surfaces That Bind Too Tightly: Can Range Separated Hybrids or DFT+U Improve Paradoxical Descriptions of Surface Chemistry? *J. Phys. Chem. Lett. just accepted,* https://doi.org/10.1021/acs.jpclett.9b01650.
85. Kulik, H. J.; Marzari, N., Transition-Metal Dioxides: A Case for the Intersite Term in Hubbard-Model Functionals. *J. Chem. Phys.* **2011,** *134*, 094103.
86. Chertihin, G. V.; Bare, W. D.; Andrews, L., Reactions of Laser-Ablated Chromium Atoms with Dioxygen. Infrared Spectra of CrO, OCrO, CrOO, CrO 3, Cr (OO) 2, Cr 2 O 2, Cr 2 O 3 and Cr 2 O 4 in Solid Argon. *J. Chem. Phys.* **1997,** *107*, 2798-2806.
87. Chertihin, G. V.; Andrews, L., Reactions of Laser-Ablated Manganese Atoms with Dioxygen. Infrared Spectra of MnO, OMnO, Mn (O2),(MnO) 2, and Higher Oxide Complexes in Solid Argon. *J. Phys. Chem. A* **1997,** *101*, 8547-8553.
88. Gutsev, G. L.; Rao, B.; Jena, P.; Li, X.; Wang, L.-S., Experimental and Theoretical Study of the Photoelectron Spectra of MnO X−(X= 1–3) Clusters. *J. Chem. Phys.* **2000,** *113*, 1473-1483.
89. Chertihin, G. V.; Saffel, W.; Yustein, J. T.; Andrews, L.; Neurock, M.; Ricca, A.; Bauschlicher, C. W., Reactions of Laser-Ablated Iron Atoms with Oxygen Molecules in

Condensing Argon. Infrared Spectra and Density Functional Calculations of Iron Oxide Product Molecules. *J. Phys. Chem.* **1996,** *100*, 5261-5273.
90. Andrews, L.; Chertihin, G. V.; Ricca, A.; Bauschlicher, C. W., Reactions of Laser-Ablated Iron Atoms with Oxygen Molecules: Matrix Infrared Spectra and Density Functional Calculations of OFeO, FeOO, and Fe (O2). *J. Am. Chem. Soc.* **1996,** *118*, 467-470.
91. Danset, D.; Alikhani, M. E.; Manceron, L., Reactivity of Atomic Cobalt with Molecular Oxygen: A Combined IR Matrix Isolation and Theoretical Study of the Formation and Structure of CoO2. *J. Phys. Chem. A* **2005,** *109*, 97-104.
92. Chertihin, G. V.; Citra, A.; Andrews, L.; Bauschlicher, C. W., Reactions of Laser-Ablated Cobalt Atoms with O2. Infrared Spectra of Cobalt Oxides in Solid Argon. *J. Phys. Chem. A* **1997,** *101*, 8793-8802.
93. Citra, A.; Chertihin, G. V.; Andrews, L.; Neurock, M., Reactions of Laser-Ablated Nickel Atoms with Dioxygen. Infrared Spectra and Density Functional Calculations of Nickel Oxides NiO, ONiO, Ni2O2, and Ni2O3, Superoxide NiOO, Peroxide Ni (O2), and Higher Complexes in Solid Argon. *J. Phys. Chem. A* **1997,** *101*, 3109-3118.
94. Campo Jr, V. L.; Cococcioni, M., Extended DFT+ U+ V Method with on-Site and Inter-Site Electronic Interactions. *J. Phys.: Condens. Matter* **2010,** *22*, 055602.
95. Wagner, L. K., Types of Single Particle Symmetry Breaking in Transition Metal Oxides Due to Electron Correlation. *J. Chem. Phys.* **2013,** *138*, 094106.
96. Launila, O., Spectroscopy of CrF: Rotational Analysis of the A6Σ+-X6Σ+ Band System in the 1-μm Region. *J. Mol. Spectrosc.* **1995,** *169*, 373-395.
97. Koivisto, R.; Wallin, S.; Launila, O., Spectroscopy of CrF: Extension of Rotational Analysis of the A6Σ+-X6Σ+ Band System. *J. Mol. Spectrosc.* **1995,** *172*, 464-468.
98. Wenthold, P. G.; Gunion, R. F.; Lineberger, W., Ultraviolet Negative-Ion Photoelectron Spectroscopy of the Chromium Oxide Negative Ion. *Chem. Phys. Lett.* **1996,** *258*, 101-106.
99. Gordon, R.; Merer, A., Rotational and Hyperfine Structure in the A6Σ+–X 6Σ+ Electronic Transition of MnO. *Can. J. Phys.* **1980,** *58*, 642-656.
100. Merer, A. J., Spectroscopy of the Diatomic 3d Transition Metal Oxides. *Annu. Rev. Phys. Chem.* **1989,** *40*, 407-438.
101. Aguirre, F.; Husband, J.; Thompson, C. J.; Stringer, K. L.; Metz, R. B., The Low-Lying Electronic States of FeO+: Rotational Analysis of the Resonance Enhanced Photodissociation Spectra of the 6 Π 7/2← X 6 Σ+ System. *J. Chem. Phys.* **2003,** *119*, 10194-10201.
102. Halfen, D.; Ziurys, L. M., Millimeter/Submillimeter Velocity Modulation Spectroscopy of FeO+ (X 6σ+): Characterizing Metal Oxide Cations. *Chem. Phys. Lett.* **2010,** *496*, 8-13.
103. Metz, R. B.; Nicolas, C.; Ahmed, M.; Leone, S. R., Direct Determination of the Ionization Energies of FeO and CuO with VUV Radiation. *J. Chem. Phys.* **2005,** *123*, 114313.
104. Neese, F., The ORCA Program System. *Wiley Interdiscip. Rev.: Comput. Mol. Sci.* **2012,** *2*, 73-78.
105. Perdew, J. P.; Burke, K.; Ernzerhof, M., Generalized Gradient Approximation Made Simple. *Phys. Rev. Lett.* **1996,** *77*, 3865.
106. Weigend, F.; Ahlrichs, R., Balanced Basis Sets of Split Valence, Triple Zeta Valence and Quadruple Zeta Valence Quality for H to Rn: Design and Assessment of Accuracy. *Phys. Chem. Chem. Phys.* **2005,** *7*, 3297-3305.
107. Adamo, C.; Barone, V., Toward Reliable Density Functional Methods without Adjustable Parameters: The PBE0 Model. *J. Chem. Phys.* **1999,** *110*, 6158-6170.

108. Eckert, F.; Pulay, P.; Werner, H. J., Ab Initio Geometry Optimization for Large Molecules. *J. Comput. Chem.* **1997,** *18*, 1473-1483.
109. Schlegel, H. B., In *Advances in Chemical Physics: Ab Initio Methods in Quantum Chemistry, Part I*, Lawley, K. P., Ed. John Wiley and Sons.: 1987; Vol. 67, p 249.
110. Schlegel, H. B., In *Modern Electronic Structure Theory*, Yarkony, D. R., Ed. Yarkony, D. R.: 1995; p 459.
111. Schlegel, H. B., In *Encyclopedia of Computational Chemistry*, v. R. Schleyer, P., Ed. John Wiley and Sons.: 1998.
112. Horn, H.; Weiß, H.; Háser, M.; Ehrig, M.; Ahlrichs, R., Prescreening of Two-Electron Integral Derivatives in SCF Gradient and Hessian Calculations. *J. Comput. Chem.* **1991,** *12*, 1058-1064.
113. Baker, J., An Algorithm for the Location of Transition States. *J. Comput. Chem.* **1986,** *7*, 385-395.
114. Kendall, R. A.; Dunning Jr, T. H.; Harrison, R. J., Electron Affinities of the First-Row Atoms Revisited. Systematic Basis Sets and Wave Functions. *J. Chem. Phys.* **1992,** *96*, 6796-6806.
115. Woon, D. E.; Dunning Jr, T. H., Gaussian Basis Sets for Use in Correlated Molecular Calculations. III. The Atoms Aluminum through Argon. *J. Chem. Phys.* **1993,** *98*, 1358-1371.
116. Jiang, W.; DeYonker, N. J.; Wilson, A. K., Multireference Character for 3d Transition-Metal-Containing Molecules. *J. Chem. Theory Comput.* **2012,** *8*, 460-468.
117. Lee, T. J.; Taylor, P. R., A Diagnostic for Determining the Quality of Single-Reference Electron Correlation Methods. *Int. J. Quantum Chem.* **1989,** *36*, 199-207.
118. Lee, T. J.; Rice, J. E.; Scuseria, G. E.; Schaefer, H. F., Theoretical Investigations of Molecules Composed Only of Fluorine, Oxygen and Nitrogen: Determination of the Equilibrium Structures of FOOF,(NO) 2 and FNNF and the Transition State Structure for FNNF Cis-Trans Isomerization. *Theor. Chim. Acta* **1989,** *75*, 81-98.
119. Janssen, C. L.; Nielsen, I. M., New Diagnostics for Coupled-Cluster and Møller–Plesset Perturbation Theory. *Chem. Phys. Lett.* **1998,** *290*, 423-430.
120. Karton, A.; Daon, S.; Martin, J. M., W4-11: A High-Confidence Benchmark Dataset for Computational Thermochemistry Derived from First-Principles W4 Data. *Chem. Phys. Lett.* **2011,** *510*, 165-178.
121. Lu, T.; Chen, F., Multiwfn: A Multifunctional Wavefunction Analyzer. *J. Comput. Chem.* **2012,** *33*, 580-592.
122. Sherrill, C. D.; Krylov, A. I.; Byrd, E. F.; Head-Gordon, M., Energies and Analytic Gradients for a Coupled-Cluster Doubles Model Using Variational Brueckner Orbitals: Application to Symmetry Breaking in O 4+. *J. Chem. Phys.* **1998,** *109*, 4171-4181.
123. Purvis III, G. D.; Bartlett, R. J., A Full Coupled-Cluster Singles and Doubles Model: The Inclusion of Disconnected Triples. *J. Chem. Phys.* **1982,** *76*, 1910-1918.
124. Scuseria, G. E.; Schaefer III, H. F., The Optimization of Molecular Orbitals for Coupled Cluster Wavefunctions. *Chem. Phys. Lett.* **1987,** *142*, 354-358.
125. ORCA Input Library. https://sites.google.com/site/orcainputlibrary/coupled-cluster (accessed March 23, 2019).
126. Bader, R. F., A Quantum Theory of Molecular Structure and Its Applications. *Chem. Rev.* **1991,** *91*, 893-928.
127. Tang, W.; Sanville, E.; Henkelman, G., A Grid-Based Bader Analysis Algorithm without Lattice Bias. *J. Phys.: Condens. Matter* **2009,** *21*, 084204.

128. Perdew, J. P.; Parr, R. G.; Levy, M.; Balduz, J. L., Density-Functional Theory for Fractional Particle Number: Derivative Discontinuities of the Energy. *Phys. Rev. Lett.* **1982,** *49*, 1691-1694.
129. Mahler, A.; Janesko, B. G.; Moncho, S.; Brothers, E. N., When Hartree-Fock Exchange Admixture Lowers DFT-Predicted Barrier Heights: Natural Bond Orbital Analyses and Implications for Catalysis. *J. Chem. Phys.* **2018,** *148*, 244106.
130. Kulik, H. J.; Marzari, N., Systematic Study of First-Row Transition-Metal Diatomic Molecules: A Self-Consistent DFT Plus U Approach. *J. Chem. Phys.* **2010,** *133*, 114103.
131. Huber, K.-P., *Molecular Spectra and Molecular Structure: IV. Constants of Diatomic Molecules*. Springer Science & Business Media: 1979.

TOC GRAPHIC

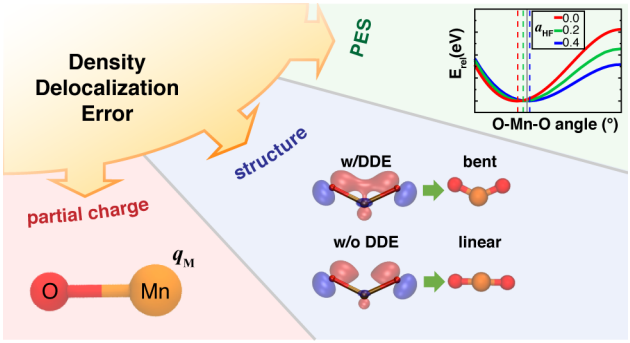
Density
Delocalization
Error
PES
E_{rel}(eV)
a_{HF}
0.0
0.2
0.4
O-Mn-O angle (°)
structure
w/DDE
bent
w/o DDE
linear
partial charge
q_M
O
Mn